JCTC Journal of Chemical Theory and Computation

Article

pubs.acs.org/JCTC

AM1 Specific Reaction Parameters for Reactions of Hydroxide Ion with Halomethanes in Complex Environments: Development and Testing

Shuai Liang and Adrian E. Roitberg*

Department of Chemistry and Quantum Theory Project, University of Florida, Gainesville, Florida 32611, United States

Supporting Information

ABSTRACT: A specific reaction parameters (SRP) approach is used to reparameterize the semiempirical AM1 method to represent two S_N2 reactions of OH^- with halomethanes (CH_3F and CH_3Cl). The objective is to develop SRP models that are able to accurately reproduce *ab initio* potential energy surfaces but with a reduction of several orders of magnitude in computational cost. The developed models, labeled AM1-SRP, have been tested in gas and aqueous phases. The results show that the AM1-SRP models are able to predict a minimum reaction path in close agreement with high level *ab initio* calculations in gas phase. A QM/MM simulation method with the solutes represented by the AM1-SRP models is used to compute the free energy profiles of the reactions in aqueous phase. The AM1-SRP models predict reaction free energies and free energy barriers in good agreement with experimental values. The current study indicates that semiempirical models may be improved to accurately reproduce an *ab initio* minimum reaction path at a considerably lower cost. The SRP approach is expected to be useful in long time scale molecular dynamics simulations where it is very expensive to use *ab initio* methods, specially in condensed phases.

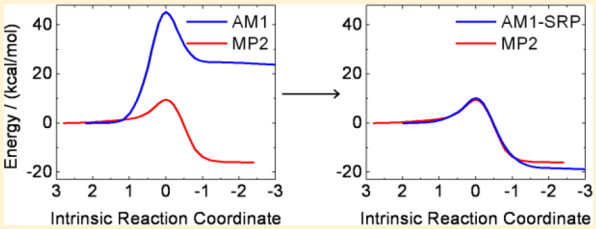

1. INTRODUCTION

Simulations of chemical reactions are very useful for interpreting experimental results and providing a microscopic understanding of the reaction mechanisms. The results of these simulations depend critically on an accurate description of the potential energy surfaces (PESs). Although an analytical functional form is possible to describe multidimensional PESs, it can only provide adequate descriptions for very simple chemical systems.[1−4] The development of accurate analytical PESs for systems involving four or more atoms has proven to be very difficult.[5−7] On the other hand, the explicit calculation of PESs using *ab initio* methods at every point needed in a dynamics study are highly time-consuming even with advanced supercomputers.[8−20] Semiempirical electronic wave functions, such as the modified neglect of diatomic overlap (MNDO),[21,22] Austin model 1 (AM1),[23,24] and parametric method 3 (PM3)[25,26] methods, are typically more than 3 orders of magnitude faster than *ab initio* methods. These semiempirical methods, however, are usually not sufficiently accurate to describe PESs with their standard parameters.

For a particular reaction or class of reactions, semiempirical models can be reparameterized to match high level *ab initio* results or experimental data. The reparameterized models, called specific reaction parameters (SRP) models,[27−29] are therefore able to represent the particular reaction(s) at an accuracy comparable to high level *ab initio* methods but with a much lower computational cost. SRP models have been developed and tested for a number of chemical and biochemical reactions.[30−43] A typical SRP model development process involves the following steps: (1) a set of molecules and/or molecular complexes related to the reaction(s) of interest are first chosen; (2) some of their structural, energetic, and other relevant properties are calculated at an *ab inito* level of theory; (3) an optimization method is used to minimize a scoring function that measures the quality of a set of trial parameters; (4) the optimized SRP model is finally tested and used for dynamics studies. A scoring function, which is crucial to the SRP model development, for the parameter optimization is usually defined as the summation of the weighted deviations of the selected molecular properties calculated by the trial parameters against *ab initio* results. A wide range of molecular properties have been considered in the development of SRP models, including molecular energies, dipole moments, bond lengths, angles, dihedrals, atomic charges, vibrational frequencies, etc.[30−43] While these SRP models represent significant improvement in comparison with the standard semiempirical models, it is not clear how to balance the weights of these properties in the scoring function for the parameter optimizations. For a particular molecular structure, even with the selected properties matching the *ab initio* results well, it may not represent the same relative position (e.g., local minima, saddle points, or other intermediate structures) on the PESs predicted by the SRP model and the *ab initio* method,[31] which introduces additional complexity into the SRP model development. Therefore, it is important for an SRP model to be able to

Received: June 6, 2013
Published: September 5, 2013

   dx.doi.org/10.1021/ct400471m | *J. Chem. Theory Comput.* 2013, 9, 4470−4480

fully characterize the PES or a region of interest for a given reaction.

In this paper, we explore the prospect of the SRP model in reproducing a minimum reaction path predicted by an *ab initio* level of theory, using a scoring function with a simple form (including only energies and forces) in the parameter optimizations. Our current work hypothesizes that the models developed for reactions in gas phase are applicable to the reactions in more complex environments and tests the developed models in aqueous solutions. Two bimolecular nucleophilic substitution (S_N2) model reactions have been selected for the current study:

$$CH_3F + OH^- \rightarrow CH_3OH + F^- \quad (R1)$$

$$CH_3Cl + OH^- \rightarrow CH_3OH + Cl^- \quad (R2)$$

Very high level *ab initio* studies of these reactions in gas phases have been carried out previously,[16,44−48] but fewer studies have addressed the microscopic mechanisms of the solvation effects on these reactions,[49−51] which are of fundamental interest and critical for design and possible improvement (the reaction rate, selectivity, etc.) of chemical reactions.[52−55] In a broader context, studying environmental effects may provide insights into a variety of reactive and catalytic processes occurring in aqueous solution and in enzymes related to chemistry, physics, and biology.[56−59]

This study aims to develop semiempirical SRP models to represent these two S_N2 reactions described above. We compare various properties of the structures along a minimum energy reaction path calculated using the SRP models and an *ab initio* method in gas phase. We compute the potentials of mean force (PMF) for the reactions in aqueous solutions using hybrid QM/MM simulations employing the umbrella sampling method.[60] The AM1 Hamiltonian[23,24] is selected to be reparameterized in the current study, although the procedure is extensible to other semiempirical models.

2. METHODOLOGIES

2.1. *Ab Initio* Calculations in Gas Phase. The reference *ab initio* data for the AM1-SRP development were calculated using the Møller−Plesset perturbation theory with the augmented correlation consistent polarized valence basis sets for double-ζ (MP2/aug-cc-pVDZ).[61] The saddle points for the two reactions were found using the synchronous transit-guided quasi-Newton (STQN) method[62,63] and were verified by a single imaginary vibrational frequency corresponding to the C atom migrating between the O and F or Cl atoms. Starting from the saddle point structure, the reactants and products were obtained by intrinsic reaction coordinate (IRC) calculations[64] using a Hessian-based Predictor−Corrector integrator algorithm.[65,66] The IRC reaction path in Cartesian coordinates (without mass-weighting) was calculated with a step size of 0.1 Bohr in each direction from the saddle point down to the reactants and products until the default convergence criteria were reached. The reactants, products, and the saddle point structures, as well as other intermediate structures generated by the IRC calculations were included in the development of the AM1-SRP parameters. The molecular geometries and energies for reactants, products, and saddle points identified at the MP2/aug-cc-pVDZ level are consistent with previous reports.[44−48] Using the standard semiempirical AM1 model, we could not locate a saddle point for reaction R2, and consequently, we could not perform the IRC calculations for this reaction. We made no extra effort in this direction. Instead, we performed AM1 calculations of various structural, energetic, or vibrational properties of the structures generated using the MP2 IRC calculations and compared these computed properties to the MP2 and AM1-SRP results. All the QM calculations in gas phase were performed using the Gaussian 09 package.[67]

2.2. Development of AM1-SRP Models. In the current study, the trial parameters for the AM1-SRP model were read in by Gaussian 09 using the keyword "input",[67] with changes up to ±20% of the standard AM1 parameters allowed. We have interfaced two optimization methods with the Gaussian 09 package[67] to optimize the parameters in a stepwise approach. A genetic algorithm (GA), as implemented in the Pyevolve package,[68] was used to optimize the parameters initially, where the optimization was performed with a population of 100 individuals uniformly distributed over the parameter space and evolved for 100 generations. Then, starting from the parameters optimized by the GA, a Levenberg−Marquardt algorithm (LMA), as implemented in the Minpack package,[69,70] was used to refine the parameters. Both GA and LMA have been demonstrated to be useful in developing SRP models previously (e.g., see refs 28, 29, 31, 71, and 72 for using of GA, and refs 30, 33, 73, and 74 for using of LMA). The current procedure combines the strength of the GA in finding a global minimum in a multiple minima problem and the LMA in finding a local minimum.

The AM1-SRP parameters are determined by minimizing the scoring function,

$$S = w_E \sum_{i=1}^{N} (E_i^{\mathrm{AM1}} - E_i^{\mathrm{MP2}})^2 + w_F \sum_{i=1}^{N} \sum_{j=1}^{M} (\vec{F}_{ij}^{\mathrm{AM1}} - \vec{F}_{ij}^{\mathrm{MP2}})^2 \quad (1)$$

where N is the number of points along the IRC (N = 53 and 52 for reaction R1 and R2, respectively), M is the number of the atoms in the system, E_i is the potential energy of the system at point i, $\vec{F}_{ij}$ is the force vector on atom j at point i, and w_E and w_F are the weight factors. For the current calculations, w_E and w_F were set to 100 $(\mathrm{Hartree})^{-2}$ and 1 $(\mathrm{Hartree/Bohr})^{-2}$, respectively. Importantly, if include only the energy term in the scoring function, the resulted parameters cannot reproduce the MP2 IRC reaction path.

Once a converged set of AM1-SRP parameters were determined, they were used in IRC calculations to see if the new model can accurately reproduce the MP2 IRC reaction path. Although the GA is very powerful in finding the global minimum in a multiple minima problem, it is not always effective for the current optimizations with 73 parameters to be adjusted simultaneously. Therefore, the combined GA and LMA fitting procedure typically needs to be repeated a few times to obtain satisfactory results (recalling the stochastic optimization nature of the GA).

2.3. QM/MM Simulations. The solute molecules were solvated in cubic boxes consisting of 1373 and 1369 water molecules for reactions R1 and R2, respectively. We included one Na^+ ion in each solvation box to neutralize the net charge (−1 e) of the reaction systems. The initial systems were heated from 0 K to a target temperature of 300 K in 50 ps with a time step of 0.5 fs, which were followed by a 50 ps equilibration

dx.doi.org/10.1021/ct400471m | J. Chem. Theory Comput. 2013, 9, 4470−4480

simulation at 300 K with a time step of 1 fs under NPT conditions with a pressure of 1.0 bar. The size of the simulation boxes is roughly 37 × 34 × 34 Å^3 after the equilibration simulations. The equilibrated systems were used as the initial configurations for the umbrella sampling calculations under NVT conditions.

The solute molecules were calculated quantum mechanically using the AM1 and AM1-SRP models, while the water molecules were represented classically by the three point TIP3P model.[75] A QM/MM-Ewald scheme[76] was used with the particle mesh Ewald method[77,78] to calculate long-range electrostatic interactions. The pressures were maintained using a weak coupling algorithm with isotropic position scaling and a relaxation time of 1 ps for NPT simulations.[79] The temperatures were maintained using Langevin dynamics with a coupling constant of 2 ps^{-1} for all the QM/MM simulations performed in this work.[80,81] Periodic boundary conditions were applied in all three Cartesian directions. The QM/MM simulations in explicit aqueous solutions were performed using the Amber 12 package.[82] The AM1-SRP models were provided through the keyword "parameter_file" in the &qmmm namelist in the Amber input file (see Supporting Information for example parameter files for Amber 12).

The one-dimensional PMFs for the reactions in TIP3P water were determined using the umbrella sampling method,[60] in order to efficiently sample the PESs. The reaction coordinate (ζ) was defined as the difference between the lengths of the breaking (C−F or C−Cl) and forming (C−O) bonds, $\zeta = d_{C-F} - d_{C-O}$ for reaction R1 and $\zeta = d_{C-Cl} - d_{C-O}$ for reaction R2. The initial configurations for umbrella sampling simulations were constructed using the steered molecular dynamics[83] to drive the reaction coordinate to the desired value within 20 ps, where the reaction coordinate, ζ, was started from −4.2 Å to 4.2 Å with a step of 0.1 Å. Seven additional windows were included around ζ = 0 Å to improve overlap between adjacent windows. Production MD simulations of 150 ps at 300 K were carried out for each window with the reaction coordinate restrained. The force constant for the harmonic potential in steered MD and production MD simulations was 100.0 kcal/mol. The PMFs along the reaction coordinate for the model reactions were estimated using a weighted histogram analysis method (WHAM).[84] The energy of the reactants in the PMF profiles is set to be zero. The convergence of the PMFs was verified by recalculating the PMF profiles using production phases of 50, 100, and 150 ps, and we found that the change in PMF profiles is less than 0.2 kcal/mol.

3. RESULTS AND DISCUSSION

This section presents our analyses and discussion of the results from the semiempirical AM1-SRP parametrizations for the reactions R1 and R2. The optimized parameters for the H, C, O, and F/Cl atoms for the two reactions are provided in Supporting Information, along with the standard AM1 parameters[23] for comparison. The average unsigned changes of the parameters are 10.2% and 10.7% for the reactions R1 and R2, respectively. The developed AM1-SRP models are able to reproduce the main features of the target reaction mechanisms, representing a significant improvement over the standard AM1 model for the description of the selected reactions.

3.1. Gas Phase Calculations. *IRC Calculations.* The parameters determined by the current fitting procedure are usually able, by construction, to reproduce rather accurately the target data (energies and forces of the selected structures along the MP2 IRC reaction path). This does not necessarily mean that the IRC using the new parameters can reproduce the MP2 IRC reaction path. A more appropriate and stringent test is to use the new parameters to run an independent IRC calculation (starting from identifying an independent saddle point structure, as described in section 2) and compare the results with the MP2 IRC reaction path. The minimum reaction paths determined by IRC calculations using MP2, AM1, and AM1-SRP methods for the two reactions are shown in Figures 1 and

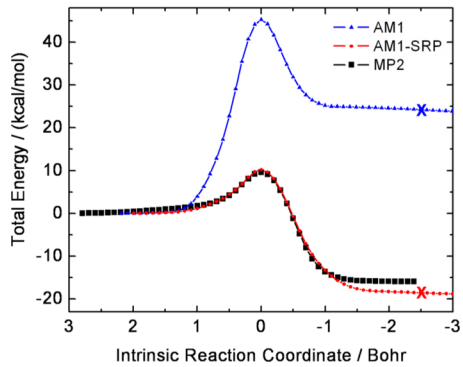

Figure 1. Total energy of the structures along IRCs calculated using the standard AM1, AM1-SRP, and MP2 models for the S_N2 reaction $CH_3F + OH^- \rightarrow CH_3OH + F^-$. The products for the AM1 and AM1-SRP models were manually selected by truncating the IRC paths (see text for details), as indicated by "X" in the figure.

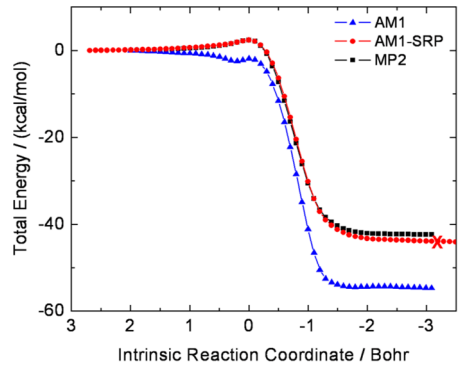

Figure 2. Total energy of the structures along IRCs calculated using the standard AM1, AM1-SRP, and MP2 models for the S_N2 reaction $CH_3Cl + OH^- \rightarrow CH_3OH + Cl^-$. Note that we could not perform an IRC calculation for this reaction using the standard AM1 model, so the AM1 energies presented here are calculated using the structures generated by MP2 IRC calculations. The products for the AM1-SRP model were manually selected by truncating the IRC path (see text for details), as indicated by "X" in the figure.

2. We note that the ion−dipole complex[44−48] is located outside of the current IRC reaction paths presented in Figures 1 and 2. Since the current work focuses on the behavior of the developed SRP Hamiltonians in solution phase where the ion-dipole minima have negligible influence on the reaction kinetics,[85,86] we did not include the ion−dipole complex or other structures outside the IRC reaction paths for the parameter fitting.

From Figure 1, we can see that the standard AM1 model fails to describe the exothermic nature of reaction R1, as will be detailed later. In addition, the standard AM1 model predicts a

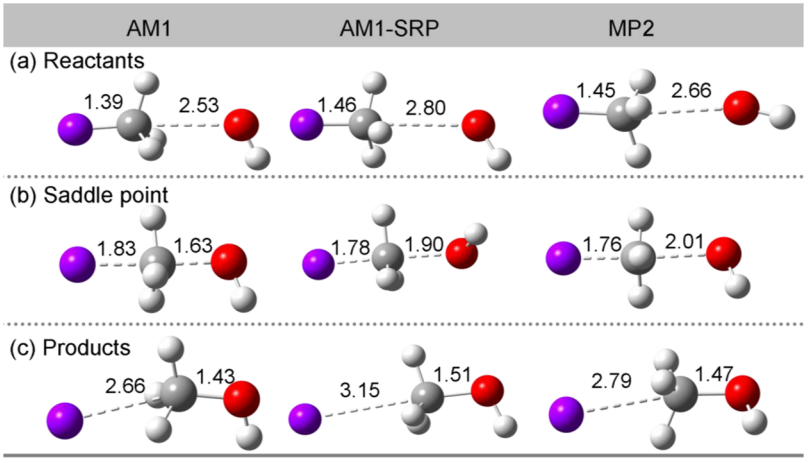

Figure 3. Geometries of the reactants, saddle point, and products of the S_N2 reaction $CH_3F + OH^- \rightarrow CH_3OH + F^-$, as identified by IRC calculations using the standard AM1, AM1-SRP, and MP2 models. The H, C, O, and F atoms are represented by white, gray, purple, and red spheres, respectively. The C−F and C−O bond distances (in Å) are indicated in the legend.

much higher reaction barrier for this reaction. In comparison with the standard AM1 model, the current AM1-SRP model improved significantly in reproducing the MP2 IRC reaction path. The overall agreement between the MP2 and AM1-SRP results is rather impressive for the entire reaction path. For the reverse direction (from the saddle point to the reactants) of the IRC, the deviation of the AM1-SRP from MP2 IRC results is not clearly discernible. In the forward direction (from the saddle point to the products) of the reaction, the IRC calculation using the AM1 or the current AM1-SRP model did not yield the products determined by the MP2 method. Inspection of the molecular structures along the IRC shows that the product F^- ion formed a bond to the H atom of the OH group of the product CH_3OH, which is reasonable for the current gas phase calculations. Further optimization of the MP2 products also generate similar configurations (the default displacement convergence criterion of IRC calculations is relatively larger than that of optimization calculations using Gaussian 09 package[67]). These configurations are not likely to form in aqueous phase due to the screening effect of the coulomb interactions by water molecules. In addition, it is well-known that some semiempirical methods are not able to accurately model the long-range interactions, due to the use of minimal basis sets.[87] A number of issues related to the end points used here can be traced back to this deficiency in the NDDO models. We did not make particular effort to parametrize the current AM1-SRP model to describe the interactions of the structures beyond these determined by the MP2 IRC calculations. For the following comparisons between the MP2 and AM1-SRP results in gas phase, we truncate the AM1 and AM1-SRP IRC path at the product point determined by the MP2 methods (see Figure 1) and use the truncated structure as the AM1-SRP products (which will be presented and discussed later).

Figure 2 shows the results of the IRC calculations using the MP2, AM1, and AM1-SRP models for reaction R2. As mentioned above, we could not perform an IRC calculation for this reaction using the standard AM1 model; instead, we present AM1 single-point energies of the structures along the IRC determined using the MP2 method. The AM1 model fails to predict a reaction barrier, and it predicts a much larger reaction energy, while the AM1-SRP model improved significantly in reproducing the MP2 IRC results. The agreement between the MP2 and the AM1-SRP results is very good for the entire reaction path. The AM1-SRP model cannot predict the structures of the products for this reaction as well, forming a similar configuration (here the Cl^- ion formed a bond with the H atom of the OH group of the product CH_3OH) as described for reaction R1. We again truncate the AM1-SRP IRC reaction path at the product point determined using the MP2 method for the following comparisons (Figure 2).

Geometries. In Figures 3 and 4, the AM1 and AM1-SRP geometries of the reactants, saddle points, and products from the IRC calculations for the two reactions are presented in comparison with MP2 geometries. Two important geometrical parameters, the distances of C−O and C−F or C−Cl, for the current S_N2 reactions are indicated in the figures. Other geometrical parameters (C−H bond length, O−H bond length, O−C−F/Cl bond angles, etc.) are not shown since both AM1 and AM1-SRP models perform rather well in predicting these values.

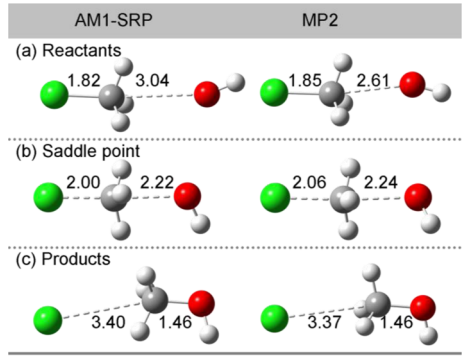

Figure 4. Geometries of the reactants, saddle point, and products of the S_N2 reaction $CH_3Cl + OH^- \rightarrow CH_3OH + Cl^-$, as identified by IRC calculations using the AM1-SRP and MP2 models. The Cl atoms are represented by green spheres, and other atoms are represented and colored as in Figure 3. The C−Cl and C−O bond distances (in Å) are indicated in the legend. Note that we could not perform an IRC calculation for this reaction with the standard AM1 model; therefore, AM1 structures are not available for comparison.

dx.doi.org/10.1021/ct400471m | J. Chem. Theory Comput. 2013, 9, 4470−4480

Figure 3 shows the geometries determined using the three different methods for reaction R1. For the reactants (Figure 3a), the standard AM1 model predicts a shorter C−F bond length of 1.39 Å for the CH_3F molecule comparing to that of 1.45 Å, as determined using the MP2 method. The AM1-SRP model predicts a C−F bond length of 1.46 Å, which is rather close to the MP2 results. For the C−O distance of the reactants, the AM1 model predicts a value of 2.53 Å while the AM1-SRP model predicts a value of 2.80 Å, comparing to the MP2 value of 2.66 Å. We note both the AM1 and AM1-SRP C−O distances should be considered acceptable since the PES at this range of C−O distances is very flat. For the saddle point geometries (Figure 3b), the AM1 model predicts a much longer C−F (1.83 Å) and shorter C−O (1.63 Å) distances comparing to those observed (1.76 Å for C−F and 2.01 for C−O) in the MP2 saddle point geometry. AM1-SRP performs much better than the standard AM1 model, yielding quite accurate saddle point geometries (1.78 Å for C−F and 1.90 for C−O) for this model reaction. Both the AM1 and AM1-SRP models fail in predicting the geometries of the products, as mentioned above. Nevertheless, the AM1 and AM1-SRP geometries of the products truncated from the IRC are reasonably close to the MP2 geometries (Figure 3c).

Figure 4 shows the geometries of the reactants, saddle point, and products for reaction R2. Since we could not carry out an IRC calculation for this reaction using the AM1 model, only the MP2 and AM1-SRP geometries are presented in Figure 4 for comparison. For the reactants (Figure 4a), the MP2 model predicts that the oxygen atom binds to one hydrogen atom (top H atom in Figure 4a, with a distance of 2.33 Å) of the methyl group. The AM1-SRP model predicts a somewhat longer C−O distance for the reactants. The AM1-SRP reactants geometries should be considered acceptable since the PES around the C−O distances is very flat. The AM1-SRP model predicts a C−Cl distance remarkably well in comparison with MP2 results for the reactants. At the saddle point (Figure 4b), the C−Cl distance and the C−O distance is only 0.06 and 0.02 Å, respectively, shorter than those determined at the MP2 level. The AM1-SRP geometries of the products truncated from IRC calculations are nearly the same as the MP2 geometries (Figure 4c).

For both reactions, the OH^- group approaches the central carbon atom with the oxygen, carbon, and fluorine/chlorine atoms close but not strictly linear (Figure 3a and 4a). The Walden inversion (inversion of the original CH_3 configuration) takes place after the saddle point (Figure 3b and 4b). The AM1-SRP performs very well in reproducing these features of the reaction mechanisms revealed by previous reports[44−48] as well as the current MP2 calculations.

Energies. Tables 1 and 2 show the calculated energies for the two reactions in gas phase, where the reaction energy, ΔE, and the reaction barrier height, $\Delta E^{\ddagger}$, are calculated as the difference in potential energies between the products and the reactants, and the saddle points and the reactants, respectively. Note the reactants and products here are identified by the IRC calculations (see section 2.1), and the separation of the reactant and product species can be found in Figures 3 and 4.

The AM1-SRP model performs significantly better than the AM1 model in reproducing MP2 reaction energies and reaction barrier heights. As mentioned, the AM1 model fails to describe the exothermic nature of the reaction R1, and it predicts a positive reaction energy of about 22.3 kcal/mol. The AM1-SRP model yields a reaction energy of about −18.5 kcal/mol, which is reasonably close to the MP2 reaction energy of −16.0 kcal/mol. The AM1 model also severely overestimates the reaction barrier height for this reaction. In contrast, the AM1-SRP model performs strikingly well in reproducing the MP2 reaction barrier. The computed AM1, AM1-SRP, and MP2 reaction barrier heights are 46.6 kcal/mol, 10.2 kcal/mol, and 9.6 kcal/mol, respectively (Table 1).

Table 1. Computed Reaction Energy (ΔE) and Reaction Energy Barrier ($\Delta E^{\ddagger}$) for the S_N2 Reaction $CH_3F + OH^- \rightarrow CH_3OH + F^-$ in Gas Phase (Using the AM1, AM1-SRP, and MP2 Models) and Reaction Free Energy (ΔG) and Free Energy Barrier ($\Delta G^{\ddagger}$) in TIP3P Water (Using the AM1 and AM1-SRP Models for the Solutes), along with the Experimental Values in Aqueous Phase[a]

	gas phase		aqueous phase	
	ΔE	$\Delta E^{\ddagger}$	ΔG	$\Delta G^{\ddagger}$
AM1	22.3	46.6	10.0	63.5
AM1-SRP	−18.5	10.2	−27.0	27.4
MP2	−16.0	9.6		
exp			−28.7	26.1

[a]The reactants and products in gas phase are identified by the IRC calculations (see section 2.1), while the reactants and products in the aqueous phase are over 5.6 Å from each other (see section 2.3). See the main text for the sources of experimental values. The unit of the energies is kcal/mol.

Table 2. Computed Reaction Energy (ΔE) and Reaction Energy Barriers ($\Delta E^{\ddagger}$) for the S_N2 Reaction $CH_3Cl + OH^- \rightarrow CH_3OH + Cl^-$ in Gas Phase (Using the MP2, AM1 and AM1-SRP models) and Reaction Free Energy (ΔG) and Free Energy Barrier ($\Delta G^{\ddagger}$) in TIP3P Water (Using the AM1 and AM1-SRP Models for the Solutes), along with the Experimental Values in Aqueous Phase[a]

	gas phase		aqueous phase	
	ΔE	$\Delta E^{\ddagger}$	ΔG	$\Delta G^{\ddagger}$
AM1	−54.7	−1.9	−47.2	20.1
AM1-SRP	−43.7	2.5	−32.6	33.3
MP2	−42.4	2.4		
exp			−31 ± 2	24.6

[a]The reactants and products in gas phase are identified by the IRC calculations (see section 2.1), while the reactants and products in the aqueous phase are over 5.6 Å from each other (see section 2.3). See the main text for the sources of experimental values. The unit of the energies is kcal/mol.

For the model reaction R2, the AM1 method predicts a negative barrier height using the structures determined using the MP2 method (Table 2). The AM1-SRP model predicts a barrier height of 2.5 kcal/mol, in excellent agreement with the MP2 barrier height of 2.4 kcal/mol. The AM1-SRP model also performs noticeably better in reproducing the MP2 reaction energy, where the computed AM1, AM1-SRP, and MP2 reaction energies are −54.7 kcal/mol, −43.7 kcal/mol, and −42.4 kcal/mol, respectively (Table 2).

Vibrational Frequencies. Tables 3 and 4 show the vibrational frequencies of the stationary points (reactants, saddle point, and products) using the AM1, AM1-SRP, and MP2 methods for the two model reactions. The AM1 frequency calculations were performed on the structures identified using MP2 methods since for reaction R1, the deviation of the AM1 geometries from the MP2 and AM1-SRP

Table 3. Normal Mode Harmonic Vibrational Frequencies (cm^{-1}) of the Stationary Structures for the Model Reaction $CH_3F + OH^- \rightarrow CH_3OH + F^-$, as Calculated Using the Standard AM1, AM1-SRP, and MP2 Models[a]

	reactants			saddle point			products		
mode	AM1	AM1-SRP	MP2	AM1	AM1-SRP	MP2	AM1	AM1-SRP	MP2
1	106	37	61	−841	−584	−566	−245	−23	−63
2	122	58	98	326	146	167	97	23	53
3	160	120	183	369	272	305	121	114	149
4	593	168	205	381	287	328	322	274	299
5	608	231	211	533	411	373	991	888	954
6	1059	1067	902	942	768	672	1007	946	1029
7	1072	1081	1117	1134	1064	1098	1102	1030	1088
8	1203	1088	1129	1142	1091	1122	1339	1266	1335
9	1331	1298	1392	1299	1255	1231	1340	1305	1397
10	1332	1299	1469	1310	1288	1401	1370	1310	1480
11	1370	1347	1470	1312	1292	1402	1486	1361	1482
12	3236	3114	3144	3290	3099	3178	3203	3107	3113
13	3237	3147	3272	3295	3173	3386	3225	3124	3214
14	3316	3147	3277	3297	3183	3386	3312	3135	3226
15	3388	3826	3776	3426	3858	3784	3499	3804	3846

[a]The structures determined by the MP2 model are used for the AM1 frequency calculations (see text).

Table 4. Normal Mode Harmonic Vibrational Frequencies (cm^{-1}) of the Stationary Structures for the Model Reaction $CH_3Cl + OH^- \rightarrow CH_3OH + Cl^-$, as Calculated Using the Standard AM1, AM1-SRP, and MP2 Models[a]

	reactants			saddle point			products		
mode	AM1	AM1-SRP	MP2	AM1	AM1-SRP	MP2	AM1	AM1-SRP	MP2
1	−102	59	20	−449	−393	−424	−213	−242	43
2	73	64	82	236	187	112	37	53	56
3	119	97	182	257	201	205	127	70	101
4	563	342	192	287	336	219	312	95	303
5	573	350	196	540	546	292	1032	1045	982
6	617	676	619	823	749	481	1051	1123	1043
7	830	974	968	855	988	980	1152	1163	1126
8	834	975	984	867	992	990	1342	1360	1346
9	1243	1383	1282	1134	1280	1139	1350	1382	1432
10	1330	1385	1438	1322	1353	1406	1400	1419	1486
11	1331	1390	1442	1326	1353	1410	1495	1452	1489
12	3223	3463	3159	3279	3308	3200	3193	3475	3096
13	3230	3467	3296	3285	3515	3392	3216	3479	3193
14	3301	3534	3298	3299	3516	3397	3303	3544	3214
15	3390	3748	3777	3410	3528	3780	3496	3777	3845

[a]The structures determined by the MP2 models are used for the AM1 frequency calculations (see text).

geometries are too large to make fair comparisons, and for reaction R2, we could not identify the stationary points using the AM1 method.

The imaginary frequency at the saddle point, which can be seen as a measure of the thickness of the reaction barrier,[88] shows excellent consistency with only 7% and 20% unsigned difference between the MP2 and AM1-SRP methods for the reactions R1 and R2, respectively (Tables 3 and 4), while the AM1 model predicts a higher deviation of 18% and 26% difference from the MP2 results. These results are encouraging since the vibrational properties are not explicitly included in the current fitting procedure.

The vibrational frequencies of the reactants and products calculated by the AM1-SRP model are also shown in Tables 3 and 4. For the reactants, the AM1-SRP model predicts a deviation of 12% and 30% from the MP2 values for the reactions R1 and R2, respectively, while the AM1 model predicts a higher deviation of 34% and 74% difference from the MP2 results. For the products, the AM1-SRP model predicts a deviation of 8% and 14% from the MP2 values for reactions R1 and R2, respectively, while the AM1 model predicts a higher deviation of 10% and 46% difference from the MP2 results. These calculated vibrational frequencies represent an improvement of the AM1-SRP model over the standard AM1 model. For the MP2 products of reaction R1, we see an imaginary frequency corresponding to the F atom migrating between two H atoms of the methyl group (Table 3). This occurs because the default convergence criterion of the IRC calculations is relatively large, as mentioned above, the products found here do not represent a global minimum in the PES. Similar imaginary frequencies are also observed in frequency calculations of the truncated AM1 and AM1-SRP products.

Evolution of Pertinent Bond Distances along the IRC. To further examine the ability of the current AM1-SRP parameters in describing the mechanism of the two S_N2 reactions, we have measured the evolution of pertinent bond distances for these reactions along the IRC reaction paths, as shown in Figures 5 and 6.

dx.doi.org/10.1021/ct400471m | J. Chem. Theory Comput. 2013, 9, 4470−4480

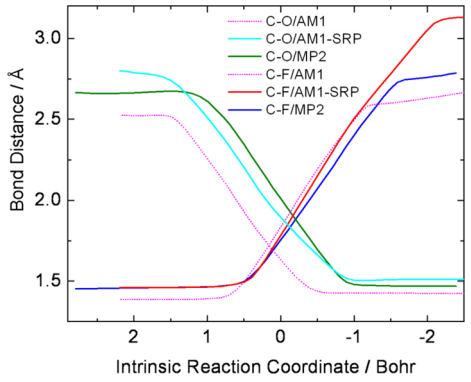

Figure 5. Evolution of the C−O and C−F bond distances along the IRCs of the S_N2 reaction $CH_3F + OH^- \rightarrow CH_3OH + F^-$, as calculated using the standard AM1, AM1-SRP, and MP2 models.

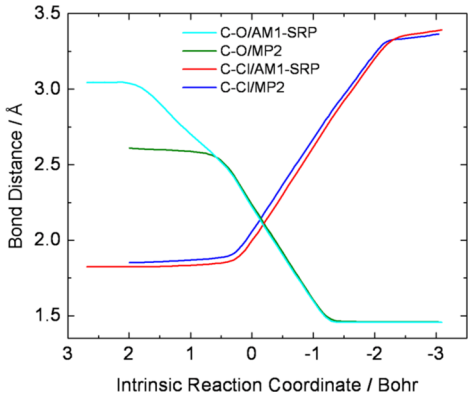

Figure 6. Evolution of the C−O and C−Cl bond distances along the IRCs of the S_N2 reaction $CH_3Cl + OH^- \rightarrow CH_3OH + Cl^-$, as calculated using the AM1-SRP and MP2 models.

Figure 5 shows the processes of the C−F bond breaking and C−O bond formation for reaction R1. We can see that as the OH^- group approaches the center carbon atom, the length of the original C−F bond remains roughly constant until the C−O bond reaches about 2.3 Å (MP2) or 2.2 Å (AM1-SRP). The C−F bond distance then starts to increase in accompany with the decreasing of the C−O bond distance, with the two bonds changing at roughly the same rate. The C−O bond is fully formed at about 1.5 Å. After this point, the C−F distance continues to increase to about 2.8 Å (MP2) and 3.1 Å (AM1-SRP). Figure 5 also shows this C−F bond breaking and C−O bond formation processes calculated using the standard AM1 model, which gives a less accurate description of the reaction mechanism.

Figure 6 shows the evolution of the distances of the bond C−Cl and C−O along the IRC, as calculated by the MP2 and AM1-SRP models. We can see that the OH group starts at a longer C−O distance by the AM1/SRP model. For the reactants determined by the MP2 model, the oxygen atom of OH^- group binds to one hydrogen atom of the central methyl group, as mentioned above (see Figure 4a). The initial bond changes correspond to the OH^- group moving away from the binding hydrogen atom toward the C_3 symmetry axis of CH_3Cl, while the C−O distance remains roughly constant. The reactants determined by the AM1-SRP model have a larger C−O distance. Again, we note that this AM1-SRP reactants geometry should be considered acceptable since the PES is very flat around these C−O distances. The C−Cl bond does not start to break until the C−O bond reaches about 2.5 Å, as predicted by both MP2 and AM1-SRP models. After this point, the C−Cl bond length then increases in accompany with the decrease of the C−O bond length, until the C−O bond is fully formed with a bond length of about 1.5 Å. The C−Cl bond continues to increase to about 3.4 Å. The MP2 and AM1/SRP models gave almost the same description of this C−Cl bond breaking and C−O bond formation processes.

3.2. Free Energy Calculations in Aqueous Phase.

Obviously, the calculation of gas phase properties using the SRP model does not save any computational cost since the model is derived from the MP2 results. The new models would be useful only if they can be applied to processes in the presence of other surrounding environment. Therefore, although the current AM1-SRP model has been developed and tested for gas-phase processes, it is critical to demonstrate that this model can be applied to condensed phase simulations. To this end, we have performed MD simulations of the model reactions in TIP3P water.[75] Umbrella sampling[60] and WHAM[84] have been used to estimate the free energy profiles of the reactions in aqueous solutions, with the solutes represented quantum-mechanically by the standard AM1 and AM1-SRP models. Since the solvents are represented via classical molecular-mechanics through the TIP3P model,[75] the possible influences of the polarization of water molecules or the proton transfer between the solute and water molecules are not considered here. The calculated PMFs for the two reactions are shown in Figures 7 and 8, respectively.

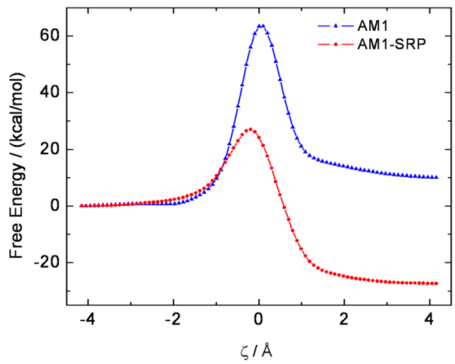

Figure 7. Computed free energy profiles for the S_N2 reaction $CH_3F + OH^- \rightarrow CH_3OH + F^-$ in aqueous phase, using the standard AM1 and AM1-SRP models. The reaction coordinate, ζ, was defined as the distance difference in the breaking (C−F) and forming (C−O) bonds, $\zeta = d_{C-F} - d_{C-O}$ (see text).

For reaction R1, the standard AM1 model predicts the reaction to be endothermic with a very high reaction barrier height of 63.5 kcal/mol (Figure 7). In contrast, the AM1-SRP model predicts a smaller barrier height of 27.4 kcal/mol, which agrees very well with the experimental value of 26.1 kcal/mol.[89] On the basis of the experimental measurements of the heat of reaction in the gas phase (−17.7 ± 2.0 kcal/mol),[90,91] the free energy of solvation of OH^- (−105.0 ± 0.5 kcal/mol),[92] CH_3F (−0.22 kcal/mol),[93] F^- (−111.1 kcal/mol),[94] and CH_3OH (−5.1 kcal/mol),[95] we obtain a free energy change of −28.7 ± 2.0 kcal/mol for the reaction in aqueous phase, which is reasonably close to our calculated value of −27.0 kcal/mol by the AM1/SRP model (also see Table 1), while the standard AM1 model failed to predict the exothermic nature of this reaction.

dx.doi.org/10.1021/ct400471m | J. Chem. Theory Comput. 2013, 9, 4470−4480

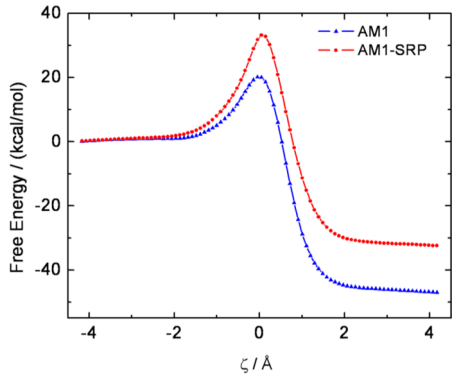

Figure 8. Computed free energy profiles for the S_N2 reaction $CH_3Cl + OH^- \rightarrow CH_3OH + Cl^-$ in aqueous phase, using the standard AM1 and AM1-SRP models. The reaction coordinate, ζ, was defined as the distance difference in the breaking (C−Cl) and forming (C−O) bonds, $\zeta = d_{C-Cl} - d_{C-O}$ (see text).

Figure 8 shows the PMF for reaction R2 obtained from the umbrella sampling MD simulations. The free energy change of this reaction calculated by the AM1 and AM1-SRP models are −47.2 and −32.6 kcal/mol, respectively. On the basis of the experimental measurements of the heat of reaction in the gas phase (−50 ± 2 kcal/mol),[46] the free energy of solvation of OH^- (−105.0 ± 0.5 kcal/mol),[92] CH_3Cl (−0.6 kcal/mol),[96] Cl^- (−81.3 kcal/mol),[94] and CH_3OH (−5.1 kcal/mol),[95] we obtain a free energy change of −31 ± 2 kcal/mol for the reaction in aqueous phase, which agrees very well with our calculated value of −32.6 kcal/mol by the AM1/SRP model, while the standard AM1 model predicts a more negative reaction energy (Table 2). The reaction free energy barrier is estimated to be 20.1 and 33.3 kcal/mol in aqueous solution by the AM1 and AM1-SRP models, respectively. The free energy barrier calculated by the AM1-SRP model is consistent with a previous QM/MM study employing a density functional method which reported a reaction barrier of 31.1 kcal/mol,[49] although an experimental value of 24.3 kcal/mol has been reported over 60 years ago.[97]

Previous calculations of similar S_N2 reactions predict a much higher reaction barrier in aqueous solutions in comparison with that in gas phases.[85,86,98−101] The current AM1-SRP models show the correct trends in the relative reactivity. The reaction barrier heights calculated in aqueous phase are about 17.2 and 30.8 kcal/mol higher for reactions R1 and R2, respectively, comparing to those calculated in gas phase (see Tables 1 and 2). The solvation has a smaller impact on the reaction barrier height of reaction R1, which might illustrate that a more electronegative fluorine atom increase the charge polarization of the saddle point structure, which is relatively more stabilized in an aqueous phase, as suggested previously.[50] Therefore, the AM1-SRP model reasonably predicts the contribution of aqueous environments on the reaction barrier heights of the model reactions.

4. CONCLUSIONS

In the current work, we developed specific reaction parameters AM1 Hamiltonians (AM1-SRP) to describe two S_N2 reactions of the hydroxide ion with halomethanes (CH_3F and CH_3Cl). We performed intrinsic reaction coordinate (IRC) calculations at the MP2 level of theory for the two reactions. Using the energies and forces of the structures along the MP2 IRCs as the target data, we reparameterized the standard AM1 model for H, C, O, and F/Cl atoms to represent the two reactions. We showed that the developed AM1-SRP models can accurately reproduce the MP2 IRC reaction path. The developed AM1-SRP models have been tested in the gas phase and demonstrated to provide comparable accuracy with respect to the MP2 results for a number of relevant properties including molecular geometries, energies, vibrational frequencies, etc. These AM1-SRP models were subsequently used in hybrid QM/MM simulations of the reactions in aqueous phase. The free energy profiles were computed with the solutes represented by the standard AM1 and AM1-SRP models. The AM1-SRP models predict reaction energies and reaction energy barriers in good agreement with the experimental data.

The current work suggests that using a scoring function with a simple form in the optimization processes, we can develop AM1-SRP models that are able to accurately reproduce a minimum reaction path calculated at the *ab initio* MP2 level of theory. We remark that the semiempirical models are typically several orders of magnitude faster than *ab initio* methods, for example, the QM/MM simulation of reaction R2 using the AM1-SRP model in the current study took about 13 days of CPU time, it would take about 18 years of CPU time if using the MP2 method to represent the solutes. Direct dynamics simulations based upon *ab initio* and DFT electronic structure theory have been performed on reactions similar to the S_N2 reactions studied in this work[11−20] and will surely become more common as time progresses. The improved semiempirical SRP models are very promising for applications involving larger systems (e.g., biomolecules, nanoparticles) and long time scale molecular dynamics simulations where the large number of energy and force evaluations needed make it extremely hard (but not impossible) to use *ab initio* methods with current computational resources.

■ ASSOCIATED CONTENT

Supporting Information

List of the optimized semiempirical parameters of AM1-SRP models, along with the standard AM1 parameters for comparison. The new AM1-SRP parameters are also provided in Gaussian 09 input and Amber 12 parameter file format. This material is available free of charge via the Internet at http://pubs.acs.org.

■ AUTHOR INFORMATION

Corresponding Author

*E-mail: rotiberg@ufl.edu.

Notes

The authors declare no competing financial interest.

■ ACKNOWLEDGMENTS

S.L. thanks Danial S. Dashti, Bill R. Miller III, and Juan B. Calabuig for their assistance in umbrella sampling simulations. S.L. also acknowledges Natali V. Di Russo, T. Dwight McGee Jr., and Bill R. Miller III for reading the original manuscript. This work was supported by National Science Foundation through Award No. CHE #0823198.

■ REFERENCES

(1) Mielke, S. L.; Peterson, K. A.; Schwenke, D. W.; Garrett, B. C.; Truhlar, D. G.; Michael, J. V.; Su, M. C.; Sutherland, J. W. H + H_2 Thermal Reaction: A Convergence of Theory and Experiment. *Phys. Rev. Lett.* **2003**, *91*, 063201.

(2) Aguado, A.; Barragan, P.; Prosmiti, R.; Delgado-Barrio, G.; Villarreal, P.; Roncero, O. A New Accurate and Full Dimensional Potential Energy Surface of H_5^+ Based on a Triatomics-in-Molecules Analytic Functional Form. *J. Chem. Phys.* **2010**, *133*, 024306.
(3) Yang, C. L.; Wang, L. Z.; Wang, M. S.; Ma, X. G. Quasi-Classical Trajectory Study of the $N(^2D) + H_2(X^1\Sigma_G^+) \rightarrow NH(X^3\Sigma^-) + H(^2S)$ Reaction Based on an Analytical Potential Energy Surface. *J. Phys. Chem. A* **2013**, *117*, 3−8.
(4) Schatz, G. C. The Analytical Representation of Electronic Potential-Energy Surfaces. *Rev. Mod. Phys.* **1989**, *61*, 669−688.
(5) Truhlar, D. G.; Steckler, R.; Gordon, M. S. Potential-Energy Surfaces for Polyatomic Reaction Dynamics. *Chem. Rev.* **1987**, *87*, 217−236.
(6) Zhang, D. H.; Collins, M. A.; Lee, S. Y. First-Principles Theory for the H + H_2O, D_2O Reactions. *Science* **2000**, *290*, 961−963.
(7) Ljubic, I.; Clary, D. C. Quasiclassical Trajectory Calculations of Hydrogen Absorption in the $(NaAlH_4)_2Ti$ System on a Model Analytical Potential Energy Surface. *Phys. Chem. Chem. Phys.* **2012**, *14*, 3915−3921.
(8) Bowman, J. M.; Czako, G.; Fu, B. N. High-Dimensional Ab Initio Potential Energy Surfaces for Reaction Dynamics Calculations. *Phys. Chem. Chem. Phys.* **2011**, *13*, 8094−8111.
(9) Bowman, J. M.; Braams, B. J.; Carter, S.; Chen, C.; Czako, G.; Fu, B.; Huang, X.; Kamarchik, E.; Sharma, A. R.; Shepler, B. C.; Wang, Y.; Xie, Z. Ab-Initio-Based Potential Energy Surfaces for Complex Molecules and Molecular Complexes. *J. Phys. Chem. Lett.* **2010**, *1*, 1866−1874.
(10) Lin, S. Y.; Zhang, P. Y.; Zhang, J. Z. H. Hybrid Many-Body-Expansion/Shepard-Interpolation Method for Constructing Ab Initio Potential Energy Surfaces for Quantum Dynamics Calculations. *Chem. Phys. Lett.* **2013**, *556*, 393−397.
(11) Li, G. S.; Hase, W. L. Ab Initio Direct Dynamics Trajectory Study of the Cl^- + CH_3Cl S_N2 Reaction at High Reagent Translational Energy. *J. Am. Chem. Soc.* **1999**, *121*, 7124−7129.
(12) Sun, L.; Hase, W. L.; Song, K. Trajectory Studies of S_N2 Nucleophilic Substitution. 8. Central Barrier Dynamics for Gas Phase Cl^- + CH_3Cl. *J. Am. Chem. Soc.* **2001**, *123*, 5753−5756.
(13) Cheon, S.; Song, K.; Hase, W. L. Central Barrier Recrossing Dynamics of the Cl^- + CD_3Cl S_N2 Reaction. *Theochem. J. Mol. Struct.* **2006**, *771*, 27−31.
(14) Sun, L. P.; Chang, E. Y.; Song, K. Y.; Hase, W. L. Transition State Dynamics and a QM/MM Model for the Cl^- + C_2H_5Cl S_N2 Reaction. *Can. J. Chem.* **2004**, *82*, 891−899.
(15) Zhang, J.; Lourderaj, U.; Sun, R.; Mikosch, J.; Wester, R.; Hase, W. L. Simulation Studies of the Cl^- + CH_3I S_N2 Nucleophilic Substitution Reaction: Comparison with Ion Imaging Experiments. *J. Chem. Phys.* **2013**, *138*, 114309.
(16) Mikosch, J.; Trippel, S.; Eichhorn, C.; Otto, R.; Lourderaj, U.; Zhang, J. X.; Hase, W. L.; Weidemuller, M.; Wester, R. Imaging Nucleophilic Substitution Dynamics. *Science* **2008**, *319*, 183−186.
(17) Sun, L. P.; Song, K. Y.; Hase, W. L. A S_N2 Reaction That Avoids Its Deep Potential Energy Minimum. *Science* **2002**, *296*, 875−878.
(18) Mikosch, J.; Zhang, J. X.; Trippel, S.; Eichhorn, C.; Otto, R.; Sun, R.; de Jong, W. A.; Weidemuller, M.; Hase, W. L.; Wester, R. Indirect Dynamics in a Highly Exoergic Substitution Reaction. *J. Am. Chem. Soc.* **2013**, *135*, 4250−4259.
(19) Zhang, J. X.; Mikosch, J.; Trippel, S.; Otto, R.; Weidemuller, M.; Wester, R.; Hase, W. L. F^- + $CH_3I \rightarrow FCH_3 + I^-$ Reaction Dynamics. Nontraditional Atomistic Mechanisms and Formation of a Hydrogen-Bonded Complex. *J. Phys. Chem. Lett.* **2010**, *1*, 2747−2752.
(20) Otto, R.; Xie, J.; Brox, J.; Trippel, S.; Stei, M.; Best, T.; Siebert, M. R.; Hase, W. L.; Wester, R. Reaction Dynamics of Temperature-Variable Anion Water Clusters Studied with Crossed Beams and by Direct Dynamics. *Faraday Discuss.* **2012**, *157*, 41−57.
(21) Dewar, M. J. S.; Thiel, W. Ground-States of Molecules. 38. MNDO Method. Approximations and Parameters. *J. Am. Chem. Soc.* **1977**, *99*, 4899−4907.
(22) Dewar, M. J. S.; Thiel, W. Ground-States of Molecules. 39. MNDO Results for Molecules Containing Hydrogen, Carbon, Nitrogen, and Oxygen. *J. Am. Chem. Soc.* **1977**, *99*, 4907−4917.
(23) Dewar, M. J. S.; Zoebisch, E. G.; Healy, E. F.; Stewart, J. J. P. AM1: A New General-Purpose Quantum-Mechanical Molecular-Model. *J. Am. Chem. Soc.* **1985**, *107*, 3902−3909.
(24) Dewar, M. J. S.; Zoebisch, E. G.; Healy, E. F.; Stewart, J. J. P. Development and Use of Quantum Mechanical Molecular Models. 76. AM1: A New General-Purpose Quantum-Mechanical Molecular-Model [erratum to document cited in CA103(2):11627f]. *J. Am. Chem. Soc.* **1993**, *115*, 5348−5348.
(25) Stewart, J. J. P. Optimization of Parameters for Semiempirical Methods 1. Method. *J. Comput. Chem.* **1989**, *10*, 209−220.
(26) Stewart, J. J. P. Optimization of Parameters for Semiempirical Methods 2. Applications. *J. Comput. Chem.* **1989**, *10*, 221−264.
(27) Pu, J. Z.; Truhlar, D. G. Tests of Potential Energy Surfaces for H +$CH_4 \rightleftarrows CH_3$+$H_2$: Deuterium and Muonium Kinetic Isotope Effects for the Forward and Reverse Reaction. *J. Chem. Phys.* **2002**, *117*, 10675−10687.
(28) Rossi, I.; Truhlar, D. G. Parameterization of NDDO Wave-Functions Using Genetic Algorithms: An Evolutionary Approach to Parameterizing Potential-Energy Surfaces and Direct Dynamics Calculations for Organic Reactions. *Chem. Phys. Lett.* **1995**, *233*, 231−236.
(29) Gonzalezlafont, A.; Truong, T. N.; Truhlar, D. G. Direct Dynamics Calculations with Neglect of Diatomic Differential-Overlap Molecular-Orbital Theory with Specific Reaction Parameters. *J. Phys. Chem.* **1991**, *95*, 4618−4627.
(30) Troya, D.; Garcia-Molina, E. Quasiclassical Trajectory Study of the $O(^3p)$ + $CH_4 \rightarrow OH + CH_3$ Reaction with a Specific Reaction Parameters Semiempirical Hamiltonian. *J. Phys. Chem. A* **2005**, *109*, 3015−3023.
(31) Nam, K.; Cui, Q.; Gao, J. L.; York, D. M. Specific Reaction Parametrization of the AM1/D Hamiltonian for Phosphoryl Transfer Reactions: H, O, and P Atoms. *J. Chem. Theory Comput.* **2007**, *3*, 486−504.
(32) Doron, D.; Major, D. T.; Kohen, A.; Thiel, W.; Wu, X. Hybrid Quantum and Classical Simulations of the Dihydrofolate Reductase Catalyzed Hydride Transfer Reaction on an Accurate Semi-Empirical Potential Energy Surface. *J. Chem. Theory Comput.* **2011**, *7*, 3420−3437.
(33) Conforti, P. F.; Braunstein, M.; Stearns, J. A.; Dodd, J. A. Collision Dynamics of $O(^3P)$ + DMMP Using a Specific Reaction Parameters Potential Form. *J. Phys. Chem. A* **2012**, *116*, 2506−2518.
(34) Yan, T. Y.; Doubleday, C.; Hase, W. L. A PM3-SRP + Analytic Function Potential Energy Surface Model for $O(^3P)$ Reactions with Alkanes. Application to $O(^3P)$ + Ethane. *J. Phys. Chem. A* **2004**, *108*, 9863−9875.
(35) Vardi-Kilshtain, A.; Major, D. T.; Kohen, A.; Engel, H.; Doron, D. Hybrid Quantum and Classical Simulations of the Formate Dehydrogenase Catalyzed Hydride Transfer Reaction on an Accurate Semiempirical Potential Energy Surface. *J. Chem. Theory Comput.* **2012**, *8*, 4786−4796.
(36) Doron, D.; Kohen, A.; Major, D. T. Collective Reaction Coordinate for Hybrid Quantum and Molecular Mechanics Simulations: A Case Study of the Hydride Transfer in Dihydrofolate Reductase. *J. Chem. Theory Comput.* **2012**, *8*, 2484−2496.
(37) Martinez, R.; Enriquez, P. A.; Puyuelo, M. P.; Gonzalez, M. Dynamics of the $O(^3P)$ + $CH_4 \rightarrow OH + CH_3$ Reaction is Similar to That of a Triatomic Reaction. *J. Phys. Chem. A* **2012**, *116*, 5026−5029.
(38) Mixcoha, E.; Garcia-Viloca, M.; Lluch, J. M.; Gonzalez-Lafont, A. Theoretical Analysis of the Catalytic Mechanism of *Helicobacter pylori* Glutamate Racemase. *J. Phys. Chem. B* **2012**, *116*, 12406−12414.
(39) Zhang, X.; Wu, R. B.; Song, L. C.; Lin, Y. C.; Lin, M. H.; Cao, Z. X.; Wu, W.; Mo, Y. R. Molecular Dynamics Simulations of the Detoxification of Paraoxon Catalyzed by Phosphotriesterase. *J. Comput. Chem.* **2009**, *30*, 2388−2401.

(40) Sherer, E. C.; York, D. M.; Cramer, C. J. Fast Approximate Methods for Calculating Nucleic Acid Base Pair Interaction Energies. *J. Comput. Chem.* **2003**, *24*, 57−67.
(41) Alhambra, C.; Wu, L.; Zhang, Z. Y.; Gao, J. L. Walden-Inversion-Enforced Transition-State Stabilization in a Protein Tyrosine Phosphatase. *J. Am. Chem. Soc.* **1998**, *120*, 3858−3866.
(42) Arantes, G. M.; Loos, M. Specific Parametrisation of a Hybrid Potential to Simulate Reactions in Phosphatases. *Phys. Chem. Chem. Phys.* **2006**, *8*, 347−353.
(43) Corchado, J. C.; EspinosaGarcia, J. Theoretical Study of the CH_4+F^- → CH_3+FH Reaction. II. Semiempirical Surfaces. *J. Chem. Phys.* **1996**, *105*, 3160−3167.
(44) Evanseck, J. D.; Blake, J. F.; Jorgensen, W. L. Ab Initio Study of the S_N2 Reactions of OH^- and OOH^- with CH_3Cl. *J. Am. Chem. Soc.* **1987**, *109*, 2349−2353.
(45) Re, S. Y.; Morokuma, K. Own N-Layered Integrated Molecular Orbital and Molecular Mechanics Study of the Reaction of OH^- with Polychlorinated Hydrocarbons $CH_{4-N}Cl_N$ (N = 2−4). *Theor. Chem. Acc.* **2004**, *112*, 59−67.
(46) Borisov, Y. A.; Arcia, E. E.; Mielke, S. L.; Garrett, B. C.; Dunning, T. H. A Systematic Study of the Reactions of OH^- with Chlorinated Methanes. 1. Benchmark Studies of the Gas-Phase Reactions. *J. Phys. Chem. A* **2001**, *105*, 7724−7736.
(47) Gonzales, J. M.; Pak, C.; Cox, R. S.; Allen, W. D.; Schaefer, H. F.; Csaszar, A. G.; Tarczay, G. Definitive Ab Initio Studies of Model S_N2 Reactions CH_3X + F^- (X = F, Cl, CN, OH, SH, NH_2, PH_2). *Chem.—Eur. J.* **2003**, *9*, 2173−2192.
(48) Sun, L. P.; Song, K. Y.; Hase, W. L.; Sena, M.; Riveros, J. A. Stationary Points for the OH^- + CH_3F → CH_3OH + F^- Potential Energy Surface. *Int. J. Mass Spectrom.* **2003**, *227*, 315−325.
(49) Hori, T.; Takahashi, H.; Nitta, T. Hybrid QM/MM Molecular Dynamics Simulations for an Ionic S_N2 Reaction in the Supercritical Water: OH^- + CH_3Cl → CH_3OH + Cl^-. *J. Comput. Chem.* **2003**, *24*, 209−221.
(50) Yin, H.; Wang, D.; Valiev, M. Hybrid Quantum Mechanical/Molecular Mechanics Study of the S_N2 Reaction of CH_3Cl + OH^- in Water. *J. Phys. Chem. A* **2011**, *115*, 12047−12052.
(51) Tucker, S. C.; Truhlar, D. G. Effect of Nonequilibrium Solvation on Chemical-Reaction Rates: Variational Transition-State-Theory Studies of the Microsolvated Reaction $Cl^-(H_2O)_N$ + CH_3Cl. *J. Am. Chem. Soc.* **1990**, *112*, 3347−3361.
(52) Kim, Y.; Cramer, C. J.; Truhlar, D. G. Steric Effects and Solvent Effects on S_N2 Reactions. *J. Phys. Chem. A* **2009**, *113*, 9109−9114.
(53) Chen, X.; Regan, C. K.; Craig, S. L.; Krenske, E. H.; Houk, K. N.; Jorgensen, W. L.; Brauman, J. I. Steric and Solvation Effects in Ionic S_N2 Reactions. *J. Am. Chem. Soc.* **2009**, *131*, 16162−16170.
(54) Acevedo, O.; Jorgensen, W. L. Exploring Solvent Effects Upon the Menshutkin Reaction Using a Polarizable Force Field. *J. Phys. Chem. B* **2010**, *114*, 8425−8430.
(55) Otto, R.; Brox, J.; Trippel, S.; Stei, M.; Best, T.; Wester, R. Single Solvent Molecules Can Affect the Dynamics of Substitution Reactions. *Nat. Chem.* **2012**, *4*, 534−538.
(56) Solvation Effects on Molecules and Biomolecules: Computational Methods and Applications. In *Solvation Effects on Molecules and Biomolecules: Computational Methods and Applications*; Canuto, S., Ed.; Springer: Dordrecht, 2008; Vol. *6*.
(57) Pierdominici-Sottile, G.; Roitberg, A. E. Proton Transfer Facilitated by Ligand Binding. An Energetic Analysis of the Catalytic Mechanism of Trypanosoma Cruzi Trans-Sialidase. *Biochemistry* **2011**, *50*, 836−842.
(58) Pierdominici-Sottile, G.; Horenstein, N. A.; Roitberg, A. E. Free Energy Study of the Catalytic Mechanism of Trypanosoma Cruzi Trans-Sialidase. From the Michaelis Complex to the Covalent Intermediate. *Biochemistry* **2011**, *50*, 10150−10158.
(59) Glowacki, D. R.; Harvey, J. N.; Mulholland, A. J. Taking Ockham's Razor to Enzyme Dynamics and Catalysis. *Nat. Chem.* **2013**, *4*, 169−176.
(60) Torrie, G. M.; Valleau, J. P. Nonphysical Sampling Distributions in Monte-Carlo Free-Energy Estimation: Umbrella Sampling. *J. Comput. Phys.* **1977**, *23*, 187−199.
(61) Moller, C.; Plesset, M. S. Note on an Approximation Treatment for Many-Electron Systems. *Phys. Rev.* **1934**, *46*, 0618−0622.
(62) Peng, C. Y.; Schlegel, H. B. Combining Synchronous Transit and Quasi-Newton Methods to Find Transition-States. *Isr. J. Chem.* **1993**, *33*, 449−454.
(63) Peng, C. Y.; Ayala, P. Y.; Schlegel, H. B.; Frisch, M. J. Using Redundant Internal Coordinates to Optimize Equilibrium Geometries and Transition States. *J. Comput. Chem.* **1996**, *17*, 49−56.
(64) Fukui, K. The Path of Chemical-Reactions—The IRC Approach. *Acc. Chem. Res.* **1981**, *14*, 363−368.
(65) Hratchian, H. P.; Schlegel, H. B. Using Hessian Updating to Increase the Efficiency of a Hessian Based Predictor-Corrector Reaction Path Following Method. *J. Chem. Theory Comput.* **2005**, *1*, 61−69.
(66) Hratchian, H. P.; Schlegel, H. B. Accurate Reaction Paths Using a Hessian Based Predictor-Corrector Integrator. *J. Chem. Phys.* **2004**, *120*, 9918−9924.
(67) Frisch, M. J. T., G. W.; Schlegel, H. B.; Scuseria, G. E.; Robb, M. A.; Cheeseman, J. R.; Scalmani, G.; Barone, V.; Mennucci, B.; Petersson, G. A.; Nakatsuji, H.; Caricato, M.; Li, X.; Hratchian, H. P.; Izmaylov, A. F.; Bloino, J.; Zheng, G.; Sonnenberg, J. L.; Hada, M.; Ehara, M.; Toyota, K.; Fukuda, R.; Hasegawa, J.; Ishida, M.; Nakajima, T.; Honda, Y.; Kitao, O.; Nakai, H.; Vreven, T.; Montgomery, Jr., J. A.; Peralta, J. E.; Ogliaro, F.; Bearpark, M.; Heyd, J. J.; Brothers, E.; Kudin, K. N.; Staroverov, V. N.; Kobayashi, R.; Normand, J.; Raghavachari, K.; Rendell, A.; Burant, J. C.; Iyengar, S. S.; Tomasi, J.; Cossi, M.; Rega, N.; Millam, J. M.; Klene, M.; Knox, J. E.; Cross, J. B.; Bakken, V.; Adamo, C.; Jaramillo, J.; Gomperts, R.; Stratmann, R. E.; Yazyev, O.; Austin, A. J.; Cammi, R.; Pomelli, C.; Ochterski, J. W.; Martin, R. L.; Morokuma, K.; Zakrzewski, V. G.; Voth, G. A.; Salvador, P.; Dannenberg, J. J.; Dapprich, S.; Daniels, A. D.; Farkas, Ö.; Foresman, J. B.; Ortiz, J. V.; Cioslowski, J.; Fox, D. J. *Gaussian 09*, Revision A.1; Gaussian, Inc.: Wallingford, CT, 2009.
(68) Perone, C. S. Pyevolve: A Python Open-Source Framework for Genetic Algorithms. *ACM SIGEVOlution* **2009**, *4*, 12−20.
(69) More, J.; Sorenson, D.; Garbow, B.; Hillstrom, K. The Minpack Project. In *Sources and Development of Mathematical Software*; Cowell, W., Ed.; Prentice-Hall: Upper Saddle River, NJ, 1984; pp 88−111.
(70) More, J.; Garbow, B.; Hillstrom, K. *User Guide for MINPACK-1*, Technical Report ANL-80-74; Argonne National Laboratory: Argonne, IL, 1980.
(71) Voityuk, A. A.; Rosch, N. AM1/D Parameters for Molybdenum. *J. Phys. Chem. A* **2000**, *104*, 4089−4094.
(72) Hutter, M. C.; Reimers, J. R.; Hush, N. S. Modeling the Bacterial Photosynthetic Reaction Center. 1. Magnesium Parameters for the Semiempirical AM1 Method Developed Using a Genetic Algorithm. *J. Phys. Chem. B* **1998**, *102*, 8080−8090.
(73) Doubleday, C. Mechanism of the Vinylcyclopropane-Cyclopentene Rearrangement Studied by Quasiclassical Direct Dynamics. *J. Phys. Chem. A* **2001**, *105*, 6333−6341.
(74) Peslherbe, G. H.; Hase, W. L. Semiempirical MNDO, AM1, and PM3 Direct Dynamics Trajectory Studies of Formaldehyde Unimolecular Dissociation. *J. Chem. Phys.* **1996**, *104*, 7882−7894.
(75) Jorgensen, W. L.; Chandrasekhar, J.; Madura, J. D.; Impey, R. W.; Klein, M. L. Comparison of Simple Potential Functions for Simulating Liquid Water. *J. Chem. Phys.* **1983**, *79*, 926−935.
(76) Nam, K.; Gao, J. L.; York, D. M. An Efficient Linear-Scaling Ewald Method for Long-Range Electrostatic Interactions in Combined QM/MM Calculations. *J. Chem. Theory Comput.* **2005**, *1*, 2−13.
(77) Darden, T.; York, D.; Pedersen, L. Particle Mesh Ewald: An N·Log(N) Method for Ewald Sums in Large Systems. *J. Chem. Phys.* **1993**, *98*, 10089−10092.
(78) Essmann, U.; Perera, L.; Berkowitz, M. L.; Darden, T.; Lee, H.; Pedersen, L. G. A Smooth Particle Mesh Ewald Method. *J. Chem. Phys.* **1995**, *103*, 8577−8593.

(79) Berendsen, H. J. C.; Postma, J. P. M.; Vangunsteren, W. F.; Dinola, A.; Haak, J. R. Molecular-Dynamics with Coupling to an External Bath. *J. Chem. Phys.* **1984**, *81*, 3684−3690.
(80) Pastor, R. W.; Brooks, B. R.; Szabo, A. An Analysis of the Accuracy of Langevin and Molecular-Dynamics Algorithms. *Mol. Phys.* **1988**, *65*, 1409−1419.
(81) Loncharich, R. J.; Brooks, B. R.; Pastor, R. W. Langevin Dynamics of Peptides—The Frictional Dependence of Isomerization Rates of N-Acetylalanyl-N′-Methylamide. *Biopolymers* **1992**, *32*, 523−535.
(82) Case, D. A.; Darden, T. A.; T.E. Cheatham, I.; Simmerling, C. L.; Wang, J.; Duke, R. E.; Luo, R.; Walker, R. C.; Zhang, W.; Merz, K. M.; Roberts, B.; Hayik, S.; Roitberg, A.; Seabra, G.; Swails, J.; Goetz, A. W.; Kolossváry, I.; Wong, K. F.; Paesani, F.; Vanicek, J.; Wolf, R. M.; Liu, J.; Wu, X.; Brozell, S. R.; Steinbrecher, T.; Gohlke, H.; Cai, Q.; Ye, X.; Wang, J.; Hsieh, M.-J.; Cui, G.; Roe, D. R.; Mathews, D. H.; Seetin, M. G.; Salomon-Ferrer, R.; Sagui, C.; Babin, V.; Luchko, T.; Gusarov, S.; Kovalenko, A.; Kollman, P. A. *Amber 12*; University of California: San Francisco, 2012.
(83) Crespo, A.; Marti, M. A.; Estrin, D. A.; Roitberg, A. E. Multiple-Steering QM-MM Calculation of the Free Energy Profile in Chorismate Mutase. *J. Am. Chem. Soc.* **2005**, *127*, 6940−6941.
(84) Kumar, S.; Bouzida, D.; Swendsen, R. H.; Kollman, P. A.; Rosenberg, J. M. The Weighted Histogram Analysis Method for Free-Energy Calculations on Biomolecules. 1. The Method. *J. Comput. Chem.* **1992**, *13*, 1011−1021.
(85) Chandrasekhar, J.; Jorgensen, W. L. Energy Profile for a Nonconcerted S_N2 Reaction in Solution. *J. Am. Chem. Soc.* **1985**, *107*, 2974−2975.
(86) Chandrasekhar, J.; Smith, S. F.; Jorgensen, W. L. S_N2 Reaction Profiles in the Gas Phase and Aqueous Solution. *J. Am. Chem. Soc.* **1984**, *106*, 3049−3050.
(87) Foster, M. E.; Sohlberg, K. Empirically Corrected DFT and Semi-Empirical Methods for Non-Bonding Interactions. *Phys. Chem. Chem. Phys.* **2010**, *12*, 307−322.
(88) Albu, T. V.; Swaminathan, S. Hybrid Density Functional Theory with a Specific Reaction Parameter: Hydrogen Abstraction Reaction of Trifluoromethane by the Hydroxyl Radical. *Theor. Chem. Acc.* **2007**, *117*, 383−395.
(89) Albery, W. J.; Kreevoy, M. M. Methyl Transfer Reactions. *Adv. Phys. Org. Chem.* **1978**, *16*, 87−157.
(90) Riveros, J. M.; Sena, M.; Guedes, G. H.; Xavier, L. A.; Slepetys, R. Recent Advances in the Energetics and Mechanisms of Gas-Phase Ionic Reactions. *Pure Appl. Chem.* **1998**, *70*, 1969−1976.
(91) Gonzales, J. M.; Allen, W. D.; Schaefer, H. F. Model Identity S_N2 Reactions $CH_3X + X^-$ (X = F, Cl, CN, OH, SH, NH_2, PH_2): Marcus Theory Analyzed. *J. Phys. Chem. A* **2005**, *109*, 10613−10628.
(92) Pliego, J. R.; Riveros, J. M. New Values for the Absolute Solvation Free Energy of Univalent Ions in Aqueous Solution. *Chem. Phys. Lett.* **2000**, *332*, 597−602.
(93) Kang, H.; Choi, H.; Park, H. Prediction of Molecular Solvation Free Energy Based on the Optimization of Atomic Solvation Parameters with Genetic Algorithm. *J. Chem Inf. Model.* **2007**, *47*, 509−514.
(94) Marcus, Y. Thermodynamics of Solvation of Ions. Part 5. Gibbs Free-Energy of Hydration at 298.15 K. *J. Chem. Soc.—Faraday Trans.* **1991**, *87*, 2995−2999.
(95) Bennaim, A.; Marcus, Y. Solvation Thermodynamics of Nonionic Solutes. *J. Chem. Phys.* **1984**, *81*, 2016−2027.
(96) Albery, W. J. The Application of the Marcus Relation to Reactions in Solution. *Annu. Rev. Phys. Chem.* **1980**, *31*, 227−263.
(97) Moelwynhughes, E. A. The Kinetics of Certain Reactions between Methyl Halides and Anions in Water. *Proc. R. Soc. Lond. A* **1949**, *196*, 540−553.
(98) Chandrasekhar, J.; Smith, S. F.; Jorgensen, W. L. Theoretical-Examination of the S_N2 Reaction Involving Chloride-Ion and Methyl-Chloride in the Gas-Phase and Aqueous-Solution. *J. Am. Chem. Soc.* **1985**, *107*, 154−163.
(99) Wang, D.; Valiev, M.; Garrett, B. C. CH_2Cl_2+OH^- Reaction in Aqueous Solution: A Combined Quantum Mechanical and Molecular Mechanics Study. *J. Phys. Chem. A* **2011**, *115*, 1380−1384.
(100) Wang, T.; Yin, H.; Wang, D.; Valiev, M. Hybrid Quantum Mechanical and Molecular Mechanics Study of the S_N2 Reaction of CCl_4 + OH^- in Aqueous Solution: The Potential of Mean Force, Reaction Energetics, and Rate Constants. *J. Phys. Chem. A* **2012**, *116*, 2371−2376.
(101) Valiev, M.; Garrett, B. C.; Tsai, M. K.; Kowalski, K.; Kathmann, S. M.; Schenter, G. K.; Dupuis, M. Hybrid Approach for Free Energy Calculations with High-Level Methods: Application to the S_N2 Reaction of $CHCl_3$ and OH^- in Water. *J. Chem. Phys.* **2007**, *127*, 051102.